Edinburgh Research Explorer

Host–Guest chemistry of self-assembled hemi-cage systems: The dramatic effect of lost pre-organization

Host–Guest chemistry of self-assembled hemi-cage systems:

The dramatic effect of lost pre-organization

Vicente Martí-Centelles, Fernanda Duarte* and Paul J. Lusby*

EaStCHEM School of Chemistry, University of Edinburgh, Joseph Black Building, David Brewster Road, Edinburgh, Scotland EH9 3FJ. Email: Paul.Lusby@ed.ac.uk, Fernanda.Duarte@ed.ac.uk

ABSTRACT: New hemi-cage compounds with the formula $Pd_2(\textbf{L1})_2(\textbf{L2})_2$ (**L1** = ditopic pyridine ligand, **L2** = bpy or TMEDA) have been synthesized and characterized by spectroscopic methods, X-ray crystallography and electronic structure methods. The host–guest chemistry of these new structures, with naphthoquinone as a guest, reveals the key role of the host shape and flexibility on competitive binding processes. The influence of counteranions, solvent and non-covalent interactions to binding were quantified by Density Functional Theory calculations. Together, this study provides new insights into the concept of pre-organized guest binding when applied to charged, coordination-assembled hosts.

INTRODUCTION

Mimicking the microenvironments of natural enzymes using simple molecular capsules has fascinated supramolecular chemists since the pioneering work of Breslow.[1] A combination of factors contributes to the remarkable activity and selectivity that many biological catalysts exhibit, which includes electrostatic preorganization[2a] of the active site through non-covalent interactions (hydrogen bonding and electrostatic) and complementary apolar environments. Conformational flexibility has also been postulated to play a key role in enzyme catalysis, wherein changes in the conformation of the enzyme or substrates result in an increase in catalytic activity.[2b] Inspired by these biological systems, a number of synthetic capsules arising from self-assembly have recently been shown to possess promising catalytic properties.[3-6] However, the rational design of preorganized but flexible supramolecu-

lar structures remains a challenge, not least because the introduction of rotors into the pre-assembly components typically produces smaller superstructures that often lack a well-defined cavity (e.g., M_2L_3 helicates). A deeper understanding of the interactions at play and their dependence on the flexibility of the host-guest complex is still lacking.

For catalytic applications, the cavities of synthetic capsules must accommodate one or two substrates. With co-ordination assemblies, reactant binding has most commonly been accomplished using the hydrophobic effect.[4-6] However, the cavities of such systems are invariably defined by large, flat aromatic surfaces and are unable to provide point electrostatic stabilization in the same way as an enzyme active. Consequently, coordination capsule catalysis has relied heavily on entropic mechanisms and/or ion-pairing effects.[4-6] Recently, we have described an alternative host-guest approach that instead exploits convergent, secondary coordination spheres as polar recognition elements.[7] The success of this method relies on minimizing competition with both the solvent and coun-teranion; the simple Pd_2L_4 cage structure, **C-1** (Scheme 1) binds complementary quinone guests most strongly as the BArF ([BArF]=B-(3,5-$(CF_3)_2C_6H_3)_4^-$) salt in dichloromethane. This approach gave some of the highest asso-ciation constants ever measured for a neutral guest with a coordination assembly, close to 10^9 M^{-1}. This polar en-capsulation mechanism also modulates the electronic properties of the guest, which has been further exploited for Diels-Alder (DA) catalysis,[8] wherein acceleration can be attributed to LUMO stabilization of the bound dieno-phile. Internal electronic activation of the dienophile selective increases reactivity compared to the bulk-phase such that the capsule microenvironment can influence both regio and chemo-selectivity. The shift from a co-encapsulation approach was also found to alleviate the long-standing problem of product inhibition.

This reaction of the bound dienophile with the incoming diene must necessarily involve some molecular re-organization of the bound species. As **C-1** is pre-organized for substrate binding, it could be anticipated that it must also undergo some conformational change to maintain contact with the both carbonyl groups at the transi-tion state (TS). Interestingly, a detailed kinetic analysis of the DA reactions showed that the effective association constant of the TS (also referred to as catalytic proficiency) is three orders of magnitude greater than the sub-strate. While part of this is likely attributable to the greater H-bond accepting strength of the TS (resulting from flow of electron density from the diene HOMO to the dienophile LUMO), the capsule must equally be able to accommodate the change in shape and size of the bound species during the reaction pathway. We were therefore keen to explore how capsule flexibility affects catalysis, targeting an evolutionary design strategy that involved

2

substituting adjacent ditopic ligands for *cis*-coordinating components (**Scheme 1**). We also anticipated that the new system would bind the same guests, allowing a direct comparison with the "full" cage. A further attractive feature of this approach is that the resultant "hemi-cage" structure should improve access of the diene to the bound dienophile. Herein we describe the synthesis of these new assemblies,[9] and describe the dramatic affect the change is structure has on host-guest chemistry, providing further insight using computational modelling.
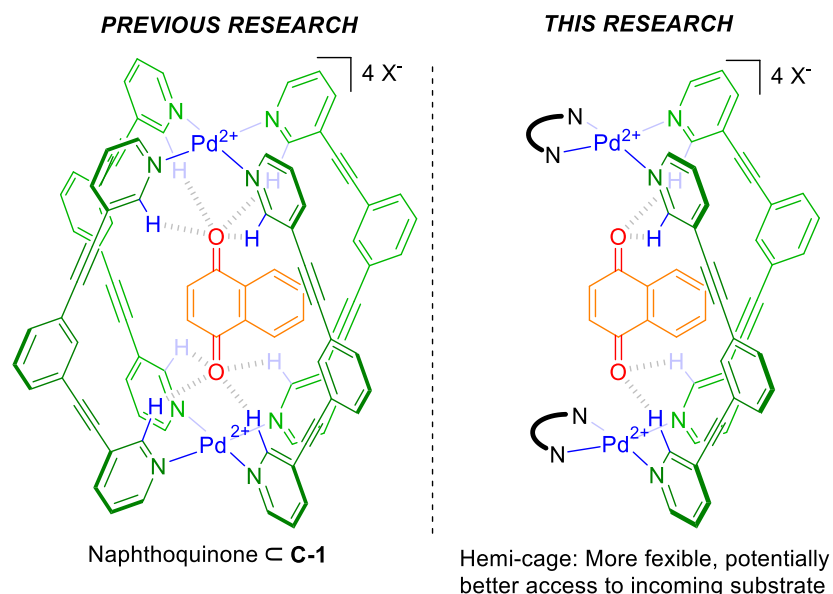
Scheme 1. Cage and hemi-cage compounds.

RESULTS AND DISCUSSION

   The hemi-cages of general formula [(*cis*-protecting ligand)Pd)$_2$(ditopic ligand)$_2$]$^{4+}$ were prepared starting with the *cis*-protect palladium(II) chloride complexes (**Scheme 2**). Following exchange of chloride for weaker interacting anions (X$^-$ = OTf$^-$, SbF$_6^-$), the self-assembly with ditopic ligands **L$^{1a/b}$** took place smoothly overnight at 60 °C in CH$_3$CN, giving **1** (X$^-$ = OTf$^-$) and **2a/b** (X$^-$ = SbF$_6^-$) in moderate to good yields. Each compound has been fully characterized as single species in solution using a combination of ^{1}H, ^{13}C and ^{19}F NMR spectroscopies, as well as HR mass spectrometry. As expected, ^{1}H DOSY revealed an increase in size following self-assembly, with similar hydrodynamic radius of 7.8 Å, 7.6 Å, and 8.3 Å calculated for **1**, **2a** and **2b**, respectively. In addition, the solid-state X-ray crystal structures confirmed the connectivity of **1** and **2b** (see below for discussion in the context of host-guest properties). Unfortunately, attempts to prepare the corresponding BArF salts using anion metathesis were unsuccessful, resulting in the formation of oils that could not be readily isolated.
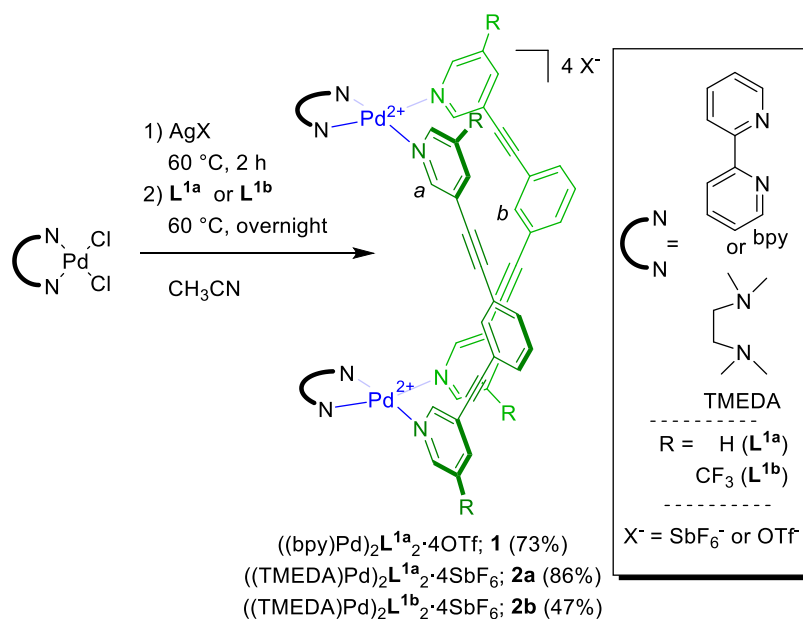
Scheme 2. Synthesis of hemi-cages 1, 2a-b. Yields of isolated assemblies shown in parenthesis.

Turning to binding studies, naphthoquinone, **G-1**, was selected as a guest, not least because comparable data for the parent cage **C-1** with a range of solvent / counteranion combinations was available.[7] Furthermore, it was also anticipated the additional favorable interactions between the inward facing C-H bonds (H$_b$) and the π-surface of **G-1** could be critical considering that half the *ortho*-pyridyl H-bond donors would be lost compared to **C-1**. Promisingly, adding a large excess of **G-1** to hemi-cage **1** produced a change in the ^{1}H NMR spectrum of the host consistent with guest binding: the signals associated with the "interior" (H$_a$ and H$_b$) both showed the largest change in chemical shift. However, a ^{1}H NMR titration between these species in CD$_3$CN (see supporting information for details) revealed very weak binding (<5 M^{-1}; **Table 1**, entry 1).

Initially, the very low affinity of **1** for **G-1** was partly attributed to effective competitive binding of the ⁻OTf anions and / or solvent, considering that **C-1** had shown relatively modest association with the same guest under comparable conditions (**Table 1**, entry 4). When attempts to explore binding in less polar solvents were hindered by the poor solubility of **1**, our attention turned to structural modifications. Unable to exchange to the preferred BArF salt (see above), we instead targeted SbF$_6$⁻ counteranions, having previously found that these inhibit quinone binding significantly less than ⁻OTf.[7] For example, the SbF$_6$⁻ salt of **C-1** binds **G-1** with a K_a of 22000 M^{-1} in CD$_3$NO$_2$, just half that of the BArF cage (**Table 1**, entry 5). We also decided to change the *cis*-protecting ligand

from bpy (2,2'-bipyrine) to TMEDA (tetramethylethylenediamine), not only expecting improved solubility, but also that the *N*-methyl groups may provide additional weak CH⋯O H-bond donors, thus regaining some of the interactions lost with removal of two ditopic ligands. However, even with these possible additional interactions and less competition from anion / solvent (SbF_6 / CD_3NO_2), the K_a of hemi-cage **2a** with **G-1** was similarly low (<5 M^{-1}; **Table 1**, entry 2). It was also noted that the difference in **G-1** affinity between cage and hemi-cage structures with this less competitive counteranion / solvent combination was significantly more pronounced (**Table 1**, entries 2 vs. 5).

We also decided to investigate the CF_3 substituted ditopic ligand, **1b**, anticipating that these electron-withdrawing groups would enhance the H-bond donor strength of the *ortho*-pyridyl sites. Indeed, H_a is deshielded in the ^1H NMR spectrum of **1b** compared to the same resonance in **1a**. Similarly, a comparison of this signal in the analogous hemi-cage complexes **2a/b** also revealed downfield shifts for the CF_3 substituted variant, consistent with greater H-bond acidity. However, while titration of **G-1** into **2b** results in similar changes to the ^1H NMR spectra (deshielding of H_a indicative of increased H-bonding; significant upfield shifting of H_b ($\Delta\delta > 0.6$ ppm), consistent with the formation of CH⋯π interactions), these changes occurred only gradually with a large excess of guest (**Figure 1**). Indeed, fitting to a 1:1 binding isotherm revealed only a slight increase (compared to **1** and **2a**) in affinity, with a K_a of just 21 M^{-1} (**Table 1**, entry 3).
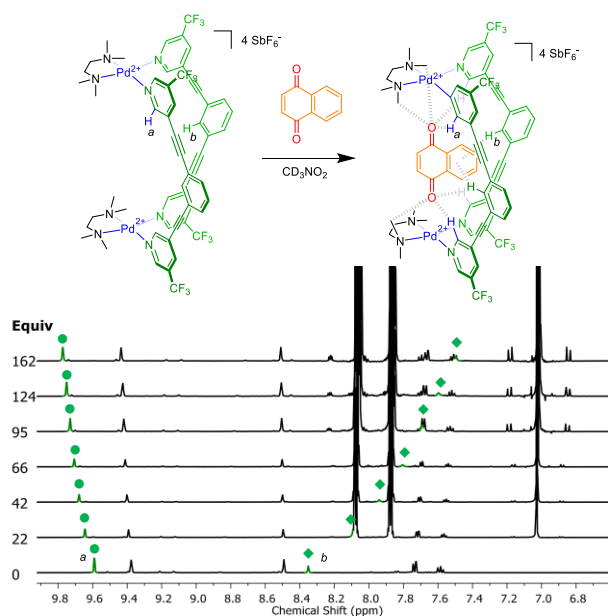
Figure 1. Partial ^{1}H NMR spectra (500 MHz, CD_3NO_2, 300 K) for the titration of hemi-cage, **2b** with naphtho-quinone, **G-1**.

Table 1. Comparison of association constants, K_a, for hemi-cage (1a, 2a, 2b) and cage (C-1) systems with naphthoquinone guest, G-1 (300 K).

Entry	Host	Counter-anion	Solvent	K_a (M^{-1})
1	**1**	$^-$OTf	CD_3CN	<5
2	**2a**	SbF_6^-	CD_3NO_2	<5
3	**2b**	SbF_6^-	CD_3NO_2	21
4	**C-1**	$^-$OTf	CD_3CN	210 [a]
5	**C-1**	SbF_6^-	CD_3NO_2	22000 [a]
5	**C-1**	BArF	CD_2Cl_2	3.5×10^5 [a]

[a] From ref [7]. Errors estimated to be less than 10%.
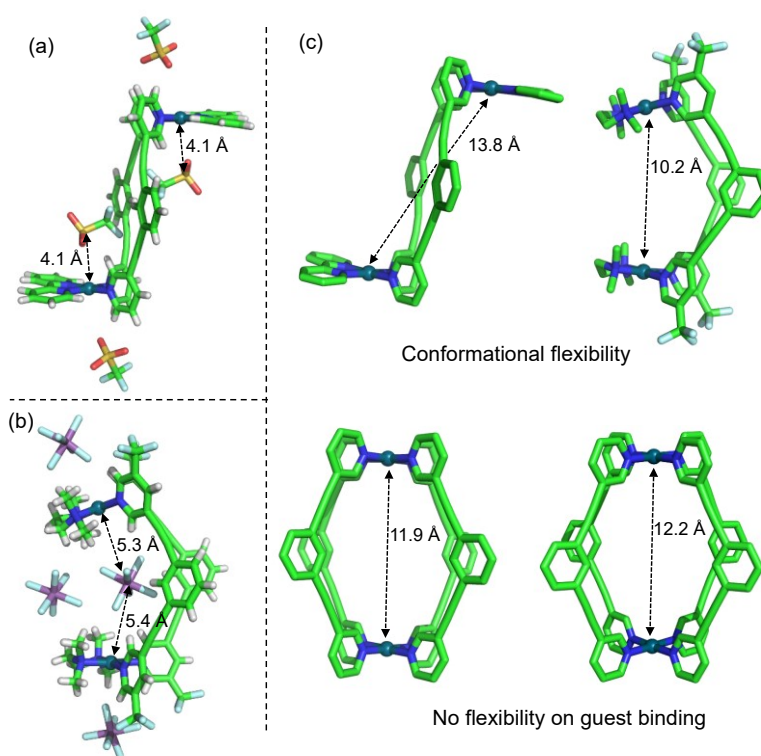
Figure 2. X ray crystal structures of (a) hemi-cage **1a**·4OTf; (b) hemi-cage **2b**·4SbF$_6$. (c) Comparison of confor-mational flexibility between hemi-cage and cage systems (guest and counterions removed for clarity). In the case of hemi-cages, the two structures (**1a**·4OTf, top left; **2b**·4SbF$_6$, top right) show significantly different global con-

6

formations (chair vs boat). In comparison, the two cage structures (**C-1·4OTf**, bottom left; pentacenedione⊂**C-1·4OTf**, bottom right) exhibit very little structural change. Pd-anion and Pd-Pd distances in Å.

While we were unable to co-crystalize any of the host-guest complexes, perhaps unsurprising because of their weak association, we obtained X-ray crystallographic quality single crystals of "free" hemi-cage systems **1a** and **2b** (**Figure 2**). Notably, the solid-state structures reveal significant global differences—whereas **1a** crystallizes in a transoid ("chair") conformation, with a Pd-Pd distance of nearly 14 Å, **2b** adopts a cisoid ("boat") orientation, with just over 10 Å between Pd ions (**Figure 2a**). In the case of **1a**, we find that there are $^-$OTf anions residing above and below each (bipy)Pd(pyidyl)$_2$$^{2+}$ primary coordination sphere, forming close contacts with both inward and outward facing *ortho*-pyridyl H-atoms. In the case of **2b**, a single SbF_6^- anion is located within the hemi-cage "cavity", forming multiple short contacts with both the "upper" and "lower" inward-facing *ortho*-pyridyl and TMEDA *N*-Me hydrogen atoms. We should also note that the average Pd-N($\mathbf{L^{1a}}$) bond lengths in structure **1a** (2.02 Å) are very similar to the Pd-N($\mathbf{L^{1a}}$) bond lengths in the parent **C-1** cage (2.03 Å), suggesting there is minimal electronic perturbation by the *cis*-protecting bpy ligand (i.e. *trans*-influence), which could have potentially affected the (C)H-bond donor strength (the average Pd-N(bpy) bond lengths are also similar, 2.01 Å). As expected, the average Pd-N($\mathbf{L^{1b}}$) bond lengths in structure **2b** are slightly longer (2.05 Å), indicative of slightly weaker coordination due to the electron withdrawing CF_3 groups. However, the overall effect of the CF_3 group on the host-guest chemistry appears to be favorable (**Table 1**, entries 2 vs. 3).

An obvious question to arise is: Are the differing hemi-cage conformations conserved in solution? The single set of ^{1}H NMR signals for **1a**, **2a/b** coupled to very similar hydrodynamic radii (7.6-8.3 Å) points to a dynamic process that is fast on the NMR timescale. A more detailed, low temperature ^{1}H NMR investigation of **2a** shows that this interconversion is a low-energy process – even at 213 K, the time averaged NMR spectrum remains unchanged, except for slight broadening of the TMEDA Me signals (see Supporting Information). Considering the strength of Pd-pyridine interactions, it therefore seems likely that the "chair" and "boat" forms are readily interchangeable conformations (i.e. they interconvert through bond rotation) and not configurations. It is also likely that the "chair" and "boat" structures of **1a** and **2b** represent two likely extremes, thus we can conclude that the hemi-cage systems possess a large conformational flexibility. Significantly, this conformational flexibility is not

available to the corresponding Pd_2L_4 structure. Comparing the two known X-ray structures of cage **C-1**, they show little change in the associated Pd-Pd distances (11.9-12.2 Å, **Figure 2a**) even with quite different guests ($^-$OTf vs. pentecenedione). While the connectivity of **C-1** precludes a transoid arrangement, the conformational rigidity also prevents the "compression" necessary to maximize interactions of both H-bond donor pockets with the small single $^-$OTf anion. Such an argument would at least partly explain why the binding of **G-1** with both **2a/b** is significantly weaker than the SbF_6^- salt of **C-1**. In effect, the flexibility of **2a/b** allows SbF_6^- to form close contacts with the secondary coordination sphere of both Pd ions and thus be bound tighter. The result is that SbF_6^- displacement by **G-1** is less favorable (compared to cage **C-1**) and thus the binding constant is significantly lower.

To obtain further insights into the energetic preference and binding properties of the cage and hemi-cage systems, DFT calculations were carried out on the different host-guest structures (hosts: **C-1/1a-b/2a-b**; guests: $^-$**OTf/SbF$_6^-$/G-1**). For hosts **1** and **2**, both the cisoid and transoid conformations with substituents R=H, CF_3 (**a** and **b**, respectively) were computed. Calculations were performed at the SMD-D3(BJ)-TPSS/Def2-TZVP//D3(BJ)-TPSS/Def2-TZVP level of theory using the density fitting approximation as implemented in Gaussian 09 (version E.01).[10] The solvents used experimentally in this study— CH_3CN (ε=35.7) and CH_3NO_2 (ε=36.6) —were modeled as a continuum using the Solvation Model based on Density (SMD).[11]

In the absence of anionic guests, the calculations reveal that the cisoid ("boat") and transoid ("chair") forms of **1** and **2** are very close in energy, with the latter conformation being marginally favored, as expected based on a simple coulombic argument (**Table S9**). Furthermore, significant structural differences can be observed between the parent cage system **C-1** and even the "boat" forms of the hemi-cages **1/2**—in particular much longer Pd-Pd distances (**C-1**, 12.1Å; **1/2**, 14.6-14.9 Å; **Figure 3** and **Table S10).** Upon binding of the anionic guests ($^-$OTf and SbF_6^-), the cisoid complexes of **1/2** become more stable than the transoid form by at least 3 kcal/mol (**Table S9**). This binding also produces a significant change in the structure of the cisoid hemi-cage systems, wherein the intrinsic conformational flexibility leads to a contraction along the Pd-Pd axis of at least 5 Å for all four complexes (**Figure 3a(ii)-(iii) and b(ii)-(iii)**). Binding of the quinone guest **G-1** to cisoid forms of **1/ 2** leads to a much more subtle conformational change, with less than 1 Å reduction in the Pd-Pd distance relative to the empty cage (**Figures 3a(iv), 3b(iv)**). In contrast, binding of either neutral or anioninc guests to the parent cage **C-1** produces very

small changes in the Pd-Pd distances (**Figure 3c(ii)-(iv)**) compared to the free cage. It is also interesting to note that while **G-1** forms eight symmetric CH⋯O interactions with both the "upper" and "lower" inward-facing *ortho-* H atoms of cage **C-1 (Figure 3c(iv))**, the SbF_6^- anion sits unsymmetrically between the two sides (**Figure 4c(iii)**), as the rigid structure is unable to adopt a conformation where both pockets interact simultaneously with the guest. In the $^-$**OTf⊂C-1** complex, the asymmetric binding mode is even more pronounced, leading to an overall twisted capsule and highly asymmetric CH⋯O/F interactions (**Figure 3c(ii)** and **S36**).
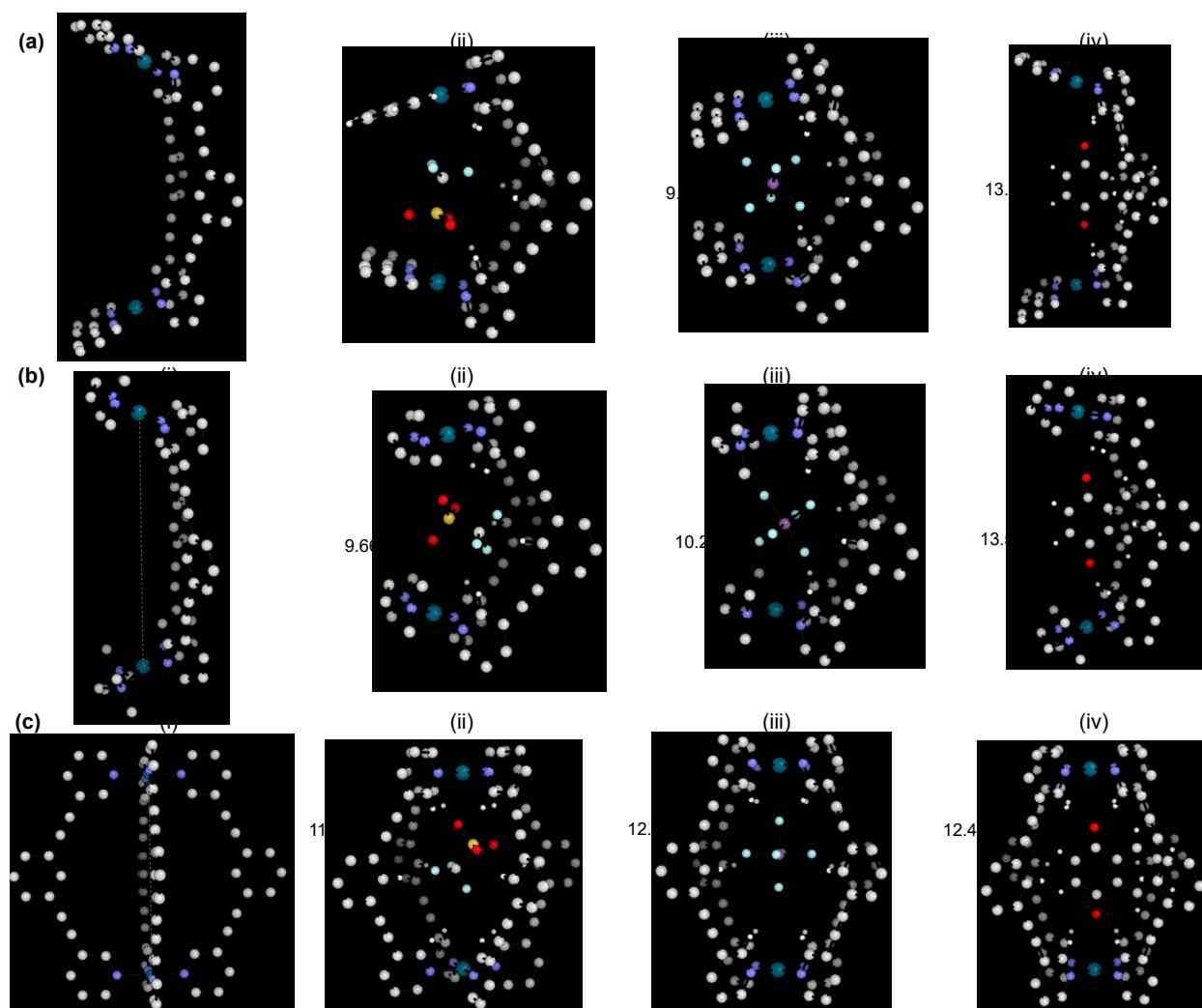
Figure 3. Optimized structures of (a) hemi-cage **1a·**, (b) hemi-cage **2a·**and (c) cage **C-1·**systems in (i) the absence and with (ii), OTf⁻, (iii) SbF_6^- and (iv) **G-1** guests at the D3(BJ)-TPSS/Def2-TZVP level of theory in the gas phase. Structures for empty hemi-cage **1a/b** and **2a/bb** in their cisoid ("boat") and transoid ("chair") forms are presented in **Figure S35**.

Next, we compared the binding energies of the different guest species to **C-1**, **1a/b** and **2a/b**. From an experimental point of view, the previously reported BArF salt of **C-1** best embodies an anion free cavity, and thus provides a useful benchmark against which *in silico* host-guest results can be compared. Significantly, we observe a good correlation between the measured value for **G-1** in dichloromethane ($K_a = 3.5 \times 10^5$ M^{-1}; $\Delta G = -7.6$ kcal mol^{-1}) and the computed values in dichloromethane ($\varepsilon = 8.9$; $\Delta G = -9.9$ kcal mol^{-1}, see **Table S11**). In CH$_3$CN ($\varepsilon = 35.7$) and CH$_3$NO$_2$ ($\varepsilon = 36.6$) the computed association energies decrease to -7.6 and -7.9 kcal mol^{-1}, respectively, which compare well to experimental values of -4.4 and -6.4 kcal mol^{-1}, respectively. Even though calculations systematically overestimate the experimental values, they match well the experimentally observed trends. Such tendency to overbind has been previously recognized when using the TPSS-D3(BJ) functional to study the Kr$_2$ and benzene-methane complexes.[12] This suggests that dispersion effects may be slightly overestimated by the empirical dispersion term used in combination with this functional. Moreover, our model does not explicitly take into account the interactions of the solvent with the host and guest, which might explain the discrepancy between absolute values. Further studies of this topic will be the subject of future work.
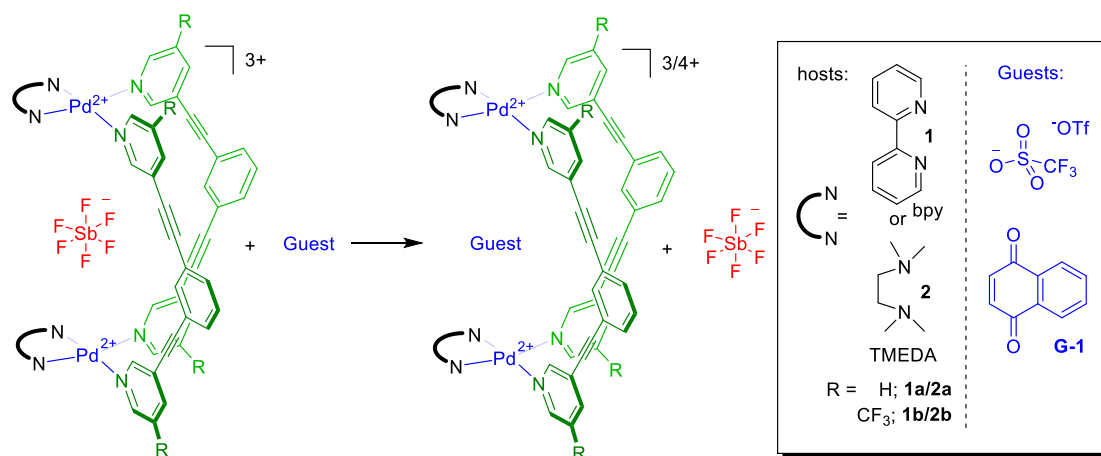
Favorable non-covalent interactions (NCI) between the guest and the cavity can be identified by computing the NCI index[13] (**Figure 4**). The NCI analysis, which is computed based on the gradient of density of each system, confirms the presence of attractive CH···O interactions between the host's inward facing *o*-pyridyl CH groups and the quinone oxygens, as well as interactions from the "equatorial" CH group of the host with the π-surface of the **G-1**. This is consistent with upfield shifting of H$_b$ observed through NMR ($\Delta\delta > 0.6$ ppm, **Figure 1**).
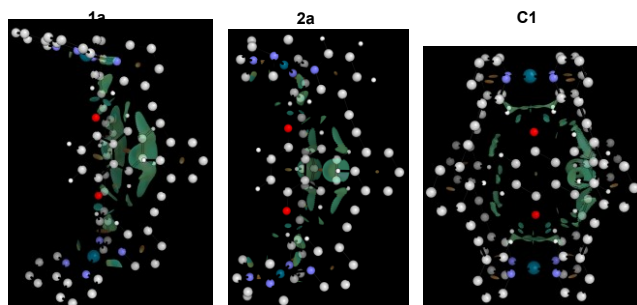
Figure 4: Non Covalent Interaction (NCI) isosurfaces of the optimized host-guest complex. Geometries were optimized at the D3(BJ)-TPSS/Def2-TZVP level of theory in gas phase.

Compared to **C-1**, binding of **G-1** to hosts **1** and **2** is less favorable. For **2a** the host-guest binding free energies is −3.4 kcal mol⁻¹ in CH₃CN, while for **1a** it is actually endothermic (+0.2 kcal mol⁻¹ in CH₃CN; −0.1 kcal mol⁻¹ in CH₃NO₂, **Table S11**). These results lead to the question about the origin of the differences in binding between **1** and **2** and suggest that even in the absence of counterions these systems show intrinsically different behaviour, with binding of **G1** to **1a** being intrinsically unfavourable. Analysis of the electron distribution (**Table S13**) provides evidence that in **C-1** the host-guest complex is much more polarised than in **1a/2a**. This is due to not only the more acid character of the CH groups in **C1** but also to the less negative net charge on the Pd centres compared to **1a/2a**, which will reduce the electron repulsion between the Pd and the oxygen atoms of the guest. In fact, NBO analysis suggests a favorable interaction between the oxygen atoms and the metal center (**Table S14**). In both cases, the addition of electron withdrawing CF₃ groups gives a slightly more favourable binding, as it increases the acidity of the CH groups.

Table 2: Computed binding free energies (in kcal mol⁻¹) at the SMD[CH₃CN]-D3(BJ)-TPSS/Def2-TZVP//D3(BJ)-TPSS/Def2-TZVP level of theory.

Guest	1a ΔH	$T\Delta S$	ΔG	1b ΔH	$T\Delta S$	ΔG	2a ΔH	$T\Delta S$	ΔG	2b ΔH	$T\Delta S$	ΔG	C-1 ΔH	$T\Delta S$	ΔG
⁻OTf	−0.1	−1.8	1.7	0.4	-3.3	3.7	−0.7	−2.2	1.5	-0.6	-3.2	2.5	2.6	2.1	0.5
G-1	4.6	−2.9	7.6	5.7	-2.1	9.8	0.9	−1.4	2.3	2.3	-2.6	4.9	−0.9	0.3	−1.2

We have also computed the competitive displacement of a bound SbF₆⁻ anion from both hemi-cage and cage systems by ⁻OTf and **G-1**. The binding free energies associated to this process are presented in **Table 2**. As can be seen, the displacement of the **SbF₆⁻** in **1a** by ⁻OTf is entropically unfavorable, while for **G-1** both enthalpic and

entropic contribution are unfavorable for binding ($\Delta G = +1.7$ for $^-$**OTf** and $\Delta G = +7.6$ kcal mol^{-1} for **G-1**). In **2a**, displacement is still unfavorable, however energies are very similar for both the anionic $^-$**OTf** and neutral **G-1** guest. In this case, enthalpic contributions are favorable for the $^-$**OTf** anion and just slightly unfavorable for **G-1**. These results reveal that, as expected, it is more difficult to remove SbF_6^- from the hemi-cage system, as the conformational flexibility allows the structure to "bite-down" more effectively on this anion, providing more non-covalent contacts. Finally, in **C-1**, binding of neutral species is enthalpically favorable relative to the anionic specie SbF_6^-, and in contrast to the previous scenarios the entropic component is almost negligible. This can be related to more favorable hydrogen bond and O-Pd interactions, which lead to a favorable enthalpic contribution.

CONCLUSIONS

The concept of utilizing rigid hosts to achieve very high binding is somewhat less favored than previously, however, we have shown here that this pattern is still true for self-assembled systems where there is excellent complementarity with the guest. While our experimental results have revealed only weak binding by these conformationally flexible hemi-cage systems, a likely result of competitive anion binding, a computational analysis has shown that these systems possess promise. We anticipate that flexible, adaptive guest binding that is difficult to achieve with rigid coordination assemblies could be particularly beneficial for stabilizing catalytic reaction pathways.

EXPERIMENTAL SECTION

Materials and methods. All reagents and solvents were purchased from Alfa Aesar, VWR or Sigma Aldrich and used without further purification unless stated otherwise. All reactions were carried out under air, unless stated otherwise. Naphthoquinone was recrystallized form hot CH_2Cl_2/pet ether 60-80 (1:3). All ^1H, ^{13}C and ^{19}F NMR spectra were recorded on either a 500 MHz Bruker AV III equipped with a DCH cryo-probe (Ava500), a 500 MHz Bruker AV IIIHD equipped with a Prodigy cryo-probe (Pro500), a 600 MHz Bruker AV IIIHD equipped with a TCI cryo-probe (Ava600) or a 400 MHz Bruker AV III equipped with BBFO+ probe (Ava400) at a constant temperature of 300 K. All DOSY experiments were performed on the Ava500 using bipolar gradient pulses for diffusion with two spoil gradients (ledbpg2s.compensated) pulse sequence. The sequence was carried out un-

der automated conditions where the duration of the magnetic field pulse gradient (δ) was 1.5 ms and the diffusion time (Δ) was 100 ms. Typically in each PFG NMR experiment, a series of 16 spectra on 32 K data points were collected and the eddy current delay (Te) was set to 5 ms in all experiments. The pulse gradients (g) were incremented from 2 to 95% of the maximum gradient strength in a linear ramp. The temperature was set and controlled at 300 K with an air flow of 400 L h^{-1} in order to avoid any temperature fluctuations due to sample heating during the magnetic field pulse gradients. Chemical shifts are reported in parts per million. Coupling constants (J) are reported uncorrected in hertz (Hz). Apparent multiplicities are reported using the following standard abbreviations: m = multiplet, q = quartet, t = triplet, d = doublet, s = singlet, bs = broad singlet. All NMR analysis was performed with MestReNova, Version 11. All assignments were made using a combination of COSY and HSQC NMR spectra (atom labeling is provided in the supporting information). MS of the cage compounds was performed on a Synapt G2 (Waters, Manchester, UK) mass spectrometer, using a direct infusion electrospray ionization source (ESI), controlled using Masslynx v4.1 software. All of the scans in the experimental are for positive ions. The samples were dissolved in acetonitrile at 50 µM. Prior to analysis, instruments were calibrated using a solution of sodium iodide (2 mg/mL) in 50:50 water:isopropanol. Capillary voltages were adjusted between 1.5 and 2.5 kV to optimize spray quality, while the sampling cone and the extraction cone voltage were minimized to reduce breakdown of the assemblies. Source temperature was set at 80 °C. The data was analyzed using the MassLynx v4.1 software.

For ^{1}H NMR titration experiments initial sample volumes were 500 µL containing 0.4–1 mM concentration of the hemi-cages (**1**, **2a** or **2b**). Solutions of naphthoquinone or solid naphthoquinone were added. ^{1}H NMR spectra (300 K) were recorded at 0–250 equivalents of quinone. Association constants were obtained by analysis of the resulting titration data using the 1:1 host–guest stoichiometry equation for fast exchange.[14]

Synthesis

2,2′-Bipyridine palladium(II) chloride[15] and *N,N,N′,N′*-tetramethylethylenediamine palladium(II) chloride[16] and ligand **L^{1a}**[17] were prepared as described in the literature.

Synthesis of ligand **L^{1b}**. Diethylamine (dried over KOH) (10 mL) was degassed with nitrogen for 10 min. Then 1,3-diethynylbenzene (114 µL, 1.11 mmol), 3-bromo-5-(trifluoromethyl)pyridine (517 mg, 2.29 mmol), PdCl$_2$(PPh$_3$)$_2$ (18 mg, 0.025 mmol) and CuI (6 mg, 0.030 mmol) were added to the reaction mixture and it was

degassed with nitrogen for 10 min. The reaction mixture was heated to 60 ºC overnight. Then, the reaction mixture was cooled to rt, EtOAc (50 mL) was added and the reaction mixture was filtered through a pad of Celite. The filtrate was washed with a saturated solution of NaHCO$_3$ (50 mL), the organic layer was dried over MgSO$_4$ and solvent was removed *in vacuo*. The solid obtained was crystallized from hot 2-propanol (40 mL), cooled to rt and further cooled in the freezer. The obtained material was filtered and washed with cold 2-propanol (5 mL) to obtain pure product as an off-white solid (305 mg, 66% yield). ^{1}H NMR (500 MHz, CDCl$_3$) δ 8.94 (s, 2H, H_a), 8.84 (s, 2H, H_b), 8.06 (s, 2H, H_c), 7.77 (t, J = 1.7 Hz, 1H, H_d), 7.59 (dd, J = 7.8, 1.6 Hz, 2H, H_e), 7.43 (t, J = 8.1 Hz, 1H, H_f) ppm. ^{13}C NMR (126 MHz, CDCl$_3$) δ 155.03, 145.37 (q, J = 3.9 Hz), 135.44 (q, J = 3.6 Hz), 134.94, 132.40, 128.93, 122.54, 126.41 – 119.39 (m), 93.15, 85.29 ppm (1 signal missing/coincidental). ^{19}F NMR (471 MHz, CDCl$_3$) δ –62.69 ppm. ESI TOF HRMS m/z: Found 417.0837 [M+H]$^+$, calculated for [C$_{22}$H$_{10}$F$_6$N$_2$+H]$^+$, 417.0821.

Synthesis of hemi-cage **1a**. A mixture of [Pd(bpy)(Cl)$_2$] (25.0 mg, 75 µmol) and AgOTf (38.5 mg, 150 µmol) in CH$_3$CN (7.5 mL) was stirred at 60 ºC for 2 h in the dark. At that time, ligand **L^{1a}** (21.2 mg, 75 µmol) was added to the reaction mixture and the reaction was stirred at 60 ºC overnight in the dark. Then, the reaction mixture was cooled to rt, filtered over a celite pad and solvent partially removed *in vacuo* (final volume of ~2 mL). The product was precipitated with Et$_2$O (10 mL), filtered and washed with Et$_2$O (10 mL) and isolated as a yellowish solid (45.9 mg, 73% yield). ^{1}H NMR (500 MHz, CD$_3$CN) δ 9.36 (d, J = 1.8 Hz, 4H, H_d), 9.08 (dd, J = 5.8, 1.5 Hz, 4H, H_e), 8.41 (d, J = 8.1 Hz, 4H, H_k), 8.33 (td, J = 7.9, 1.5 Hz, 4H, H_j), 8.24 (dt, J = 8.1, 1.6 Hz, 4H, H_f), 7.85 (t, J = 1.7 Hz, 2H, H_c), 7.76 (dd, J = 8.1, 5.7 Hz, 4H, H_g), 7.69 (dd, J = 7.8, 1.7 Hz, 4H, H_h), 7.59 – 7.50 (m, 6H, H_a+H_i), 7.35 (d, J = 5.3 Hz, 2H, H_b). ^{13}C NMR (126 MHz, CD$_3$CN) δ 157.33, 154.29, 151.42, 151.27, 144.32, 143.73, 135.72, 134.10, 130.73, 129.29, 129.02, 125.41, 125.38, 123.09, 122.11 (q, J = 320.8 Hz, OTf$^-$), 95.27, 85.35. ^{19}F NMR (471 MHz, CD$_3$CN): δ –79.21 ppm. ^{1}H DOSY NMR (500 MHz, CD$_3$CN): 7.63 × 10^{-10} m^2/s, hydrodynamic radius = 7.8 Å. ESI TOF HRMS m/z: Found 271.5287 [M–4OTf]$^{4+}$, calculated for [C$_{60}$H$_{40}$N$_8$Pd$_2$]$^{4+}$ 271.8368.

Synthesis of hemi-cage **2a**. A mixture of [Pd(TMEDA)(Cl)$_2$] (22.0 mg, 75 µmol) and AgSbF$_6$ (51.5 mg, 150 µmol) in CH$_3$CN (7.5 mL) was stirred at 60 ºC for 2 h in the dark. At that time, ligand **L^{1a}** (21.0 mg, 75 µmol) was added to the reaction mixture and the reaction was stirred at 60 ºC overnight in the dark. Then, the reaction mixture was cooled to rt, filtered over a celite pad and solvent partially removed *in vacuo* (final volume of ~2 mL). The product was precipitated with Et$_2$O (10 mL), filtered and washed with Et$_2$O (10 mL) and isolated as a

yellowish solid (62.9 mg, 86% yield). ^{1}H NMR (500 MHz, CD$_3$NO$_2$) δ 9.42 (s, 4H, H_d), 9.07 (d, J = 5.1 Hz, 4H, H_e), 8.32 (s, 2H, H_c), 8.17 (dt, J = 8.1, 1.4 Hz, 4H, H_f), 7.76 (dd, J = 8.0, 5.8 Hz, 4H, H_g), 7.66 (dd, J = 7.7, 1.5 Hz, 4H, H_b), 7.53 (t, J = 7.8 Hz, 2H, H_a), 3.29 (s, 8H, CH_2), 2.95 (s, 12H, CH_3), 2.80 (s, 12H, CH_3) ppm. ^{13}C NMR (126 MHz, CD$_3$NO$_2$) δ 153.03, 149.61, 142.36, 136.98, 132.28, 129.37, 127.71, 124.34, 122.01, 94.27, 83.92, 63.01, 50.37 ppm. ^{19}F NMR (471 MHz, CD$_3$NO$_2$) no detected signals. ^{1}H DOSY NMR (500 MHz, CD$_3$NO$_2$): 4.56 × 10^{-10} m^2/s, hydrodynamic radius = 7.6 Å. ESI TOF HRMS m/z: Found 413.7179 [M–3SbF$_6$]$^{3+}$, calculated for [C$_{52}$H$_{56}$F$_6$N$_8$Pd$_2$Sb]$^{3+}$ 413.7223. Found 738.0335 [M–2SbF$_6$]$^{2+}$, calculated for [C$_{52}$H$_{56}$F$_{12}$N$_8$Pd$_2$Sb$_2$]$^{2+}$ 738.0305.

Synthesis of hemi-cage **2b**. A mixture of [Pd(TMEDA)(Cl)$_2$] (22.0 mg, 75 μmol) and AgSbF$_6$ (51.5 mg, 150 μmol) in CH$_3$CN (7.5 mL) was stirred at 60 ºC for 2 h in the dark. At that time, ligand **L^{1b}** (31.2 mg, 75 μmol) was added to the reaction mixture and the reaction was stirred at 60 ºC overnight in the dark. Then, the reaction mixture was cooled to rt, filtered over a celite pad and solvent partially removed *in vacuo* (final volume of ~2 mL). The product was precipitated with Et$_2$O (20 mL), filtered and washed with Et$_2$O (10 mL) and isolated as a yellowish solid (39.0 mg, 47% yield). ^{1}H NMR (500 MHz, CD$_3$NO$_2$) δ 9.59 (d, J = 1.4 Hz, 4H, H_d), 9.38 (s, 4H, H_e), 8.49 (s, 4H, H_f), 8.36 (s, 2H, H_c), 7.73 (dd, J = 7.7, 1.7 Hz, 4H, H_b), 7.58 (t, J = 7.5 Hz, 2H, H_a), 3.34 (s, 8H, CH_2), 2.97 (s, 12H, CH_3), 2.85 (s, 12H, CH_3) ppm. ^{13}C NMR (126 MHz, CD$_3$NO$_2$) δ 156.37, 145.77 (q, J = 3.7 Hz), 139.70, 137.73, 132.95, 130.51 (q, J = 35.3 Hz), 129.58, 125.38, 121.58 (q, J = 273.2 Hz), 121.55, 96.50, 82.94, 63.42, 50.69, 50.66. ^{19}F NMR (471 MHz, CD$_3$NO$_2$) δ –64.43 ppm. ^{1}H DOSY NMR (500 MHz, CD$_3$NO$_2$): 4.17 × 10^{-10} m^2/s, hydrodynamic radius = 8.3 Å. ESI TOF HRMS m/z: Found 504.3656 [M–3SbF$_6$]$^{3+}$, calculated for [C$_{56}$H$_{52}$F$_{18}$N$_8$Pd$_2$Sb]$^{3+}$ 504.3721. Found 874.0128 [M–2SbF$_6$]$^{2+}$, calculated for [C$_{56}$H$_{52}$F$_{24}$N$_8$Pd$_2$Sb$_2$]$^{2+}$ 874.0053.

Single-Crystal X-ray Diffraction. Single crystals of **1** were obtained by vapour diffusion of isopropyl ether to a solution of **1** in CD$_3$CN. Single crystals of **2b** were obtained by vapour diffusion of CH$_2$Cl$_2$ to a solution of **2b** in CH$_3$NO$_2$. Suitable crystals were selected and for single-crystal using a SuperNova, Dual, Cu at zero, Atlas diffractometer. The crystal was kept at 120.00(10) K during data collection. Using Olex2,[18] the structure was solved with the ShelXT[19] structure solution program using Direct Methods and refined with the ShelXL[19] refinement package using Least Squares minimisation.

Crystal Data for **1** ($C_{64}H_{40}N_8O_{12}F_{12}S_4Pd_2$): monoclinic, space group P2$_1$/c (no. 14), a = 20.58500(13) Å, b = 14.28779(8) Å, c = 11.56733(8) Å, β = 104.8745(7)°, V = 3288.11(4) Å^3, Z = 2, T = 120.00(10) K, μ(CuKα) = 6.512 mm^{-1}, *Dcalc* = 1.699 g/cm^3, 79883 reflections measured (7.618° ≤ 2Θ ≤ 152.356°), 6863 unique (R_{int} = 0.0775, R$_{sigma}$ = 0.0232) which were used in all calculations. The final R_1 was 0.0371 (I > 2σ(I)) and wR_2 was 0.0970 (all data). CCDC 1856391 (**1a**·4OTf).

Crystal Data for **2b** ($C_{60}H_{60}Cl_8F_{36}N_8Pd_2Sb_4$): monoclinic, space group P2$_1$/c (no. 14), a = 33.4070(4) Å, b = 15.8614(2) Å, c = 16.41120(18) Å, β = 103.2985(12)°, V = 8462.80(18) Å^3, Z = 4, T = 120.00(10) K, μ(MoKα) = 2.050 mm^{-1}, *Dcalc* = 2.010 g/cm^3, 301741 reflections measured (5.526° ≤ 2Θ ≤ 59.504°), 23185 unique (R_{int} = 0.0659, R$_{sigma}$ = 0.0384) which were used in all calculations. The final R_1 was 0.0819 (I > 2σ(I)) and wR_2 was 0.1825 (all data). CCDC 1856392 (**2b**·4SbF$_6$).

Computational details All calculations have been carried out by using the GAUSSIAN 09 E.01 package.[9] The exchange functional of Tao, Perdew, Staroverov, and Scuseria (TPSS) functional[20] in conjunction with the Def2-TZVP basis sets as used with the density fitting procedure. The D3(BJ) (D3 with Becke–Johnson damping) dispersion correction[21,22] was included in all calculations. Vibrational frequencies were computed at the same level of theory to confirm the structures correspond to a minimum and to evaluate the zero-point vibrational energy (ZPVE) and thermal corrections at 298 K and 1M concentration. Vibrational entropies were corrected according to the so-called "quasi-harmonic approach[23] using a free-rotor approximation for vibrational modes below 100 cm^{-1}, and a rigid rotor approximation above this cutoff.[24] Single-point energies in solution were performed with the SMD model as an implicit solvation model using acetonitrile and nitromethane as a solvent.

Further experimental and computational details are given in the Supporting Information. Crystal data were deposited with the Cambridge Crystallographic Data Centre with numbers CCDC 1856391 (**1a**·4OTf), CCDC 1856392 (**2b**·4SbF$_6$).

ASSOCIATED CONTENT

Supporting Information

NMR spectra of the synthesized compounds, X-ray crystallography details and ^{1}H NMR titrations.

AUTHOR INFORMATION

Corresponding Author

* E-mail: Fernanda.Duarte@ed.ac.uk, Paul.Lusby@ed.ac.uk

Notes

The authors declare no competing financial interests.

REFERENCES

(1) Breslow, R.; Overman, L. E. *J. Am. Chem. Soc.* **1970**, *92*, 1075.

(2) (a) Warshel, A.; Sharma, P. K.; Kato, M.; Xiang, Y.; Liu, H.; Olsson, M. H. M.; *Chem. Rev.* **2006** *106*, 3210.

(b) Bhabha,G.; Lee, J.; Ekiert, D. C.; Gam, J.; Wilson, I. A.; Dyson, H. J.;Benkovic, S. J.; Wright, P. E.; *Science*, **2011**, 232, 234.

(3) Kang, J.; Rebek Jr., J. *Nature* **1997**, *385,* 50.

(4) Yoshizawa, M.; Takeyama, Y.; Okano, T.; Fujita, M. *J. Am. Chem. Soc.* **2003**, *125*, 3243.

(5) Hastings, C. J.; Pluth, M. D.; Bergman, R. G.; Raymond, K. N. *J. Am. Chem. Soc.* **2010**, *132*, 6938.

(6) Cullen, W.; Misuraca, M. C.; Hunter, C. A.; Williams, N. H.; M. D. Ward, *Nat. Chem.* **2016**, *8*, 231.

(7) August David, P.; Nichol Gary, S.; Lusby Paul, J. *Angew. Chem., Int. Ed.* **2016**, *55*, 15022.

(8) Marti-Centelles, V.; Lawrence, A. L.; Lusby, P. J. *J. Am. Chem. Soc.* **2018**, *140*, 2862.

(9) Fujita, M.; Ibukuro, F.; Hagihara, H.; Ogura, K. *Nature* **1994**, *367*, 720

(10) Frisch, M. J. e. a. G., Revision E.01 Gaussian Inc., Wallingford CT.

(11) Marenich, A. V.; Cramer, C. J.; Truhlar, D. G. *J. Phys. Chem. B* **2009**, *113*, 6378.

(12) Grimme, S.; Ehrlich, S.; Goerigk, L. *J. Comput. Chem.* **2011**, *32*, 1456.

(13) Johnson, E. R.; Keinan, S.; Mori-Sánchez, P.; Contreras-García, J.; Cohen, A. J.; Yang, W. *J. Am. Chem. Soc.* **2010**, *132*, 6498.

(14) Connors, K. A. *Binding Constants: The Measurement of Molecular Complex Stability*; John Wiley & Sons: New York, 1987.

(15) BaniKhaled, M. O.; Becker, J. D.; Koppang, M.; Sun, H. *Crystal Growth & Design* **2016**, *16*, 1869.

(16) Vicente, J.; Abad, J. A.; Chicote, M.-T.; Abrisqueta, M.-D.; Lorca, J.-A.; Ramírez de Arellano, M. C. *Organometallics* **1998**, *17*, 1564.

(17) Liao, P.; Langloss, B. W.; Johnson, A. M.; Knudsen, E. R.; Tham, F. S.; Julian, R. R.; Hooley, R. J. *Chem Commun.* **2010**, *46*, 4932.

(18) Dolomanov, O. V.; Bourhis, L. J.; Gildea, R. J.; Howard, J. A. K.; Puschmann, H. *J. Appl. Crystallogr.* **2009**, *42*, 339.

(19) Sheldrick, G. *Acta Cryst. A* **2015**, *71*, 3.

10(20) Tao, J.; Perdew, J. P.; Staroverov, V. N.; Scuseria, G. E. *Phys. Rev. Lett.* **2003**, *91*, 146401.

(21) Becke, A. D.; Johnson, E. R. *J. Chem. Phys.* **2005**, *123*, 154101.

(22) Johnson, E. R.; Becke, A. D. *J. Chem. Phys.* **2005**, *123*, 024101.

(23) Funes-Ardoiz, I.; Paton, R. S. **2016**.

(24) Grimme, S. *Chem. Eur. J.* **2012**, *18*, 9955.

Table of Contents Graphic

Cage

Hemi-cage

Strong interaction

Weak interaction